RSC Advances

PAPER

View Article Online
View Journal | View Issue

Cite this: *RSC Adv.*, 2021, **11**, 38605

Cation effects on the properties of halloysite-confined bis(trifluoromethylsulfonyl)imide based ionic liquids

A. V. Agafonov, L. M. Ramenskaya, E. P. Grishina and N. O. Kudryakova *

Received 16th July 2021
Accepted 22nd November 2021

DOI: 10.1039/d1ra05466j

rsc.li/rsc-advances

Four types of ionic liquids (ILs) of [X]TFSI ([X]$^+$ is a cation such as 1-butyl-3-methylimidazolium BMIm$^+$, 1-butyl-1-methylpyrrolidinium BMPyrr$^+$, 1-butyl-1-methylpiperidinium BMPip$^+$ and methyltrioctylammonium MOc$_3$Am$^+$ and TFSI$^-$ is the bis(trifluoromethylsulfonyl)imide anion) were confined in halloysite nanoclay (Hal) at an excess ionic liquid concentration (IL : Hal ~55 : 45 wt%) and studied by X-ray diffraction, TG, DSC analysis and FTIR spectroscopy. It was found that the physicochemical properties of ILs trapped by halloysite at maximum loading are similar to those of bulk ILs and change depending on the cation type and size. The cold crystallization temperature (T_{cc}) and melting point (T_m) of the crystalline mesophase in confined BMIm$^+$ and BMPyrr$^+$ ionic liquids are higher than in the bulk ones, while in the amorphous BMPyrr$^+$ mesophase, the T_{cc} and T_m values decrease by 9.7 and 14.2 °C, respectively. Confined BMPip$^+$ and MOc$_3$Am$^+$ only have the glass transition temperature (T_g), which increases by 1.5 and 8.0 °C, respectively, compared to bulk ILs. The onset decomposition temperature (T_d) decreases by 106.5, 40.7, 19.0 and 7.7 °C in BMIm$^+$, BMPip$^+$, BMPyrr$^+$ and MOc$_3$Am$^+$, respectively. The changes in the properties are explained by the cation and anion interaction with halloysite, as well as by the transformation of the ionic liquid structure. It is found that in this case the amount of the TFSI$^-$ anion *trans*-conformer increases in the following order: BMIm$^+$ > BMPyrr$^+$ ~ BMPip$^+$ >> MOc$_3$Am$^+$.

1. Introduction

Ionic liquids (ILs) – salts with a large asymmetric organic cation and a large organic/inorganic anion – are of great scientific interest due to their unique combination of physicochemical properties. ILs are characterized by a low melting point (<100 °C), absence of vapour pressure, high thermal and chemical/electrochemical stability, a wide range of density and viscosity values, ability to dissolve a lot of organic compounds and metal salts, and high polarity and ionic conductivity, which is attractive in terms of practical application of these compounds. ILs are recognized as "green" solvents for reactions of chemical synthesis, biochemical and catalytic processes, as electrolytes for energy converters and storage devices, *etc.*[1–5] It should be said that high fluidity of ionic liquids is often undesirable as it makes it more difficult to design some devices. That is why many of the practical applications require the use of thickened ionic liquids. Obtaining such ionic liquids (ionogels, IG) that would retain the characteristic properties of bulk ILs – high electric conductivity and thermal stability within a wide temperature range – is an important scientific problem.

The properties of thickened ionic liquids have been thoroughly studied by a lot of researchers in the last few years in terms of their application in catalysis, production of membranes and electrochronic materials, lubricants, encapsulation of pharmaceutical preparations, as well as in such devices as actuators and sensors, solar cells, fuel cells, double-layer capacitors, lithium batteries and others.[6–13] However, ionogels remain largely underused because their interphase structure and dynamics have not been studied well yet.[4,14–16]

Clay minerals are quite promising in terms of ionogel preparation.[17] Clay-based nanocomposites are characterized by viscoplastic properties and high electric conductivity, which allows them to be used in production of electrochemical devices. Halloysite nanotubes (HNTs) – natural clay minerals belonging to the kaolin group – are a promising type of nanomaterials that has attracted scientists' attention by its low cost, availability and biocompatibility. Besides, the large surface area and tubular structure have allowed HNTs to be applied for a variety of industrial purposes.[18] Halloysite nanotubes are successfully used as bioplastic fillers and coatings in medicine.[19–21] HNTs are an alternative to synthetic, less environmentally-friendly, toxic and expensive carbon nanotubes[22,23] and are considered applicable as adsorbents, catalysts, carriers in drug delivery systems, *etc.*[24]

G. A. Krestov Institute of Solution Chemistry of the Russian Academy of Sciences, Ivanovo, Russia. E-mail: kno@isc-ras.ru; Fax: +7-4932-336237; Tel: +7-4932-336259

Halloysite nanotubes are kaolinite scrolls with a positively charged internal aluminol surface (–Al–OH) and a negatively charged external siloxane (–Si–O–Si–) surface.[18,25] The charge separation is ensured by different values of the electric potential of the outer surface consisting of silicon dioxide tetrahedrons and inner surface made up by alumina octahedrons.[26] The chemical formula of halloysite is $Al_2Si_2O_5(OH)_4 \cdot nH_2O$, and by the hydration state halloysite nanotubes can be classified into hydrated HNTs ($Al_2Si_2O_5(OH)_4 \cdot 4H_2O$) with an interplanar d_{001} spacing of 10 Å and dehydrated HNTs ($Al_2Si_2O_5(OH)_4 \cdot 2H_2O$) with a 7 Å d_{001} spacing. The nanotubes are 0.2–1.5 μm long, and their inner and outer diameters are within the range of 10–30 nm and 40–70 nm, respectively.[27]

The large surface area (up to 60 $m^2\ g^{-1}$) and structural features of halloysite nanotubes urge to study the effects of interactions at the phase interface and confinement on the properties of ionic liquid molecules in limited ionogel spaces. It is known that the structure of ILs in ionogels undergoes considerable changes in comparison with bulk ILs making them up. Interactions at the solid–liquid interface largely determine ionogel properties. Ionic liquids are capable of self-aggregation and microheterogeneity due to their unusual structure and amphiphilic nature.[28] The structural organization of ILs in ionogels leads to the formation of ordered layers and unusual properties of ionic liquids near the phase interface.[29–31]

The properties of ionogels are largely dependent on the confinement phenomenon – restrictions of molecular mobility of ionic liquid molecules as a result of interaction with the nanoparticle surface and their inclusion in the nanocavities of porous fillers.[9,28,32–34] The phenomenon of ionic liquid confinement, when ion–wall interactions become more important than ion–ion interactions in the bulk may cause changes in ionic liquid physicochemical properties.[32] Interactions of ionic liquid ions with the nanoparticle surface transform the primary structure of the initial ionic liquids into lamellar structures consisting of alternating layers formed by cations and anions, the location of which depends on the surface charge sign of the nanoparticles, their shape and size determining the charge density.[35] The layers made up by cations and anions are repeated in the ionogel bulk over a large distance from the filler particle surface (tens of nanometers). The interactions between the cation and anion layers determined by the polarization and association effects are hindered by the interpermeation of the anions and cations into the mesophases from the hydrocarbon chains. This results in the formation of cationic and anionic channels in the ionogels.[36]

IL/HNT nanocomposites have a wide range of potential applications in production of plastics,[37–42] quasi-solid electrolytes for supercapacitors, secondary batteries,[28,43] *etc.*, since they can have high ionic conductivity with a large proportion of the reinforcing component.[44–46] We have previously shown[46] that ionogels based on coagulation structures of halloysite in bis(trifluoromethylsulfonyl) imide ILs with cations $EMIm^+$, $BMIm^+$, BM_2Im^+, $BMPyrr^+$, $BMPip^+$ and MOc_3Am^+ could be classified as pseudoplastic fluids of the Bingham type. The fluidity of these ionogels linearly correlates with the dynamic viscosity and molar volumes of pure ionic liquids, and the temperature dependence of the ionic conductivity of ionogels in the range from −20 to +80 °C obeys the Vogel–Fulcher–Tamman equation. The formation of a stabilizing ionic solvation shell on the surface of filler particles is a factor that affects interparticle interactions in ionogels.

The aim of this work was to identify the regularities of confinement effects in ionogels on the properties of ionic liquids with the same hydrophobic bis(trifluoromethylsulfonyl) imide anion and different cations ($BMIm^+$, $BMPyrr^+$, $BMPip^+$ and MOc_3Am^+) immobilized on halloysite nanotubes. Limitations and confinement observed in ionogels affect the temperatures of phase transitions of ionic liquids, their thermal stability, conformational transformations of immobilized ions, hydration state and supramolecular structure of halloysite.

2. Experimental part

2.1. Materials

The following ionic liquids were used in this work:

– 1-Butyl-3-methylimidazolium bis(trifluoromethylsulfonyl) imide BMImTFSI (Aldrich, ≥98%, CAS:174899-83-30); the water impurity content was 0.035 wt%;

– 1-Butyl-1-methylpyrrolidinium bis(trifluoromethylsulfonyl) imide BMPyrrTFSI (MerkKGaA, high purity, CAS: 223437-11-4); the water impurity content was 0.04 wt%;

– 1-Butyl-1-methylpiperidinium bis(trifluoromethylsulfonyl) imide BMPipTFSI (Aldrich, 97%, CAS: 623680-12-9;) the water impurity content was 0.064 wt%;

– Methyltrioctylammonium bis(trifluoromethylsulfonyl) imide MOc_3AmTFSI (abcr GmbH, 99%, CAS: 375395-33-8); the water impurity content was 0.12 wt%.

The ionic liquids were used without further purification. The water impurity content in the ILs given above was determined by the K. Fischer method in this work.

The structural formulae of the cations in the enumerated ionic liquids are shown in Fig. 1.

Halloysite nanoclay (Hal), $Al_2Si_2O_5(OH)_4 \cdot 2H_2O$ (Sigma-Aldrich, USA, CAS number 1332-58-7, molecular weight 294.19 g cm^{-3}, density 2.53 g cm^{-3}) was used to prepare the IL/clay composites. The elemental composition, structural and some physicochemical characteristics of the halloysite had been determined by us earlier: the length of the nanotubes can exceed 1 μm, their average outer and inner diameter are about 0.1 μm and 7.8 nm, respectively; the pore volume of 0.13 $cm^3\ g^{-1}$, particle size of 90–280 nm, surface area of 57 $m^2\ g^{-1}$ (~16 769 $m^2\ mol^{-1}$), and *Z*-potential of −13 mV.[44,45]

2.2. Preparation of ionogels

Samples of an ionic liquid and halloysite that had been kept in an LT-VO 20 vacuum drying oven (Labtex, Russia) at a temperature of 70 °C for an hour were placed into a hermetically sealed polypropylene container and mixed for 1 hour with an IKA VORTEX 4 basic vibration shaker (IKA-Werke GmbH & Co. KG, Germany). The prepared mixture was stored in an Elmasonic P30H US-bath (Elma Schmidbauer GmbH, Germany) for 2 hours, then kept in a vacuum drying oven at a temperature of

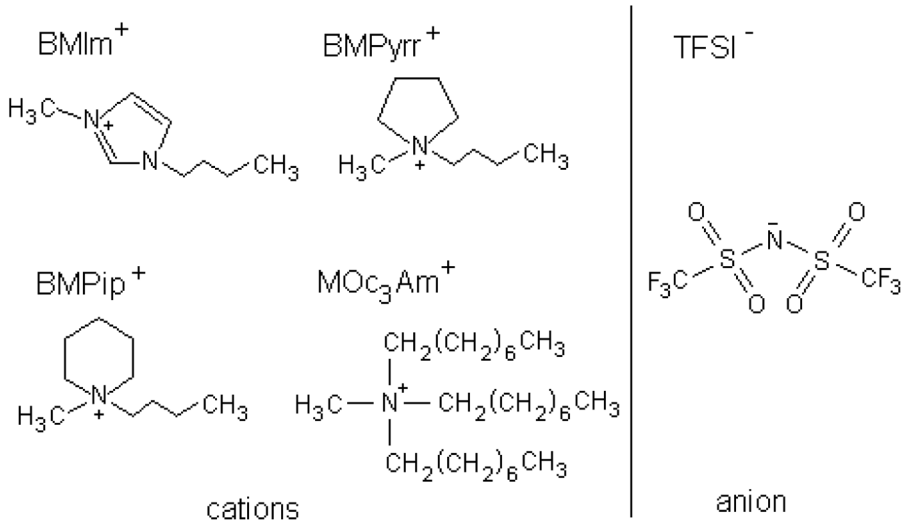

Fig. 1 Structural formulas of the cations and anion of the ionic liquids used to prepare the ionogels.

80 °C and a residual pressure of 0.1 MPa for 24 hours. The effectiveness of using vacuum to increase the loading of organic molecules into halloysite nanotubes has been confirmed in several studies.[47–49] The obtained mixture was centrifuged (on an OPn-8 desktop laboratory centrifuge, DATSAN, Russia) at a rotation speed of 6000 rpm for 45 minutes. The centrifugation in the two-phase system led to layering, after which the excess of the ionic liquid that could not be retained inside the clay was removed from the container. The prepared ionogel was saturated with the ionic liquid and retained its sedimentary stability in all the subsequent studies. The ratio of the components in the prepared composites is given in Table 1. In addition, a small amount of the obtained ionogels were washed three times with ethyl alcohol, dried in a vacuum, and then studied by FTIR spectroscopy.

2.3. Methods and apparatus

A 209 F1 Iris calorimeter (NETZSCH, Germany) was used to determine the decomposition point (T_d) of the ionic liquids, clays and composites. A 10 mg sample ~ in a platinum crucible was heated to 650 °C in an argon flow at a rate of 10 °C min^{-1}. The accuracy of the mass and temperature measurements was $\pm 10^{-6}$ g and ±0.1 °C, respectively.

A DSC 204 F1 Phoenix calorimeter (NETZSCH, Germany) was employed to measure the thermodynamic parameters, such as temperatures of melting (T_m), crystallization (T_c), glass transition (T_g) and (ΔH) phase transition enthalpy. A 10 mg sample~ in a hermetically sealed Al capsule was cooled by liquid nitrogen to −120 °C at a rate of 10 °C min^{-1} and then heated to 100 °C at a rate of 10 °C min^{-1}. The measurements

Table 1 Composition of the ionogels prepared by halloysite saturation with different ionic liquids

IL concentration in the ionogel	Ionic liquid cation			
	$BMIm^+$	$BMPyrr^+$	$BMPip^+$	MOc_3Am^+
α, wt%	55.2	55.7	54.8	56.3
C, mol/100 g IG	0.131	0.132	0.126	0.086

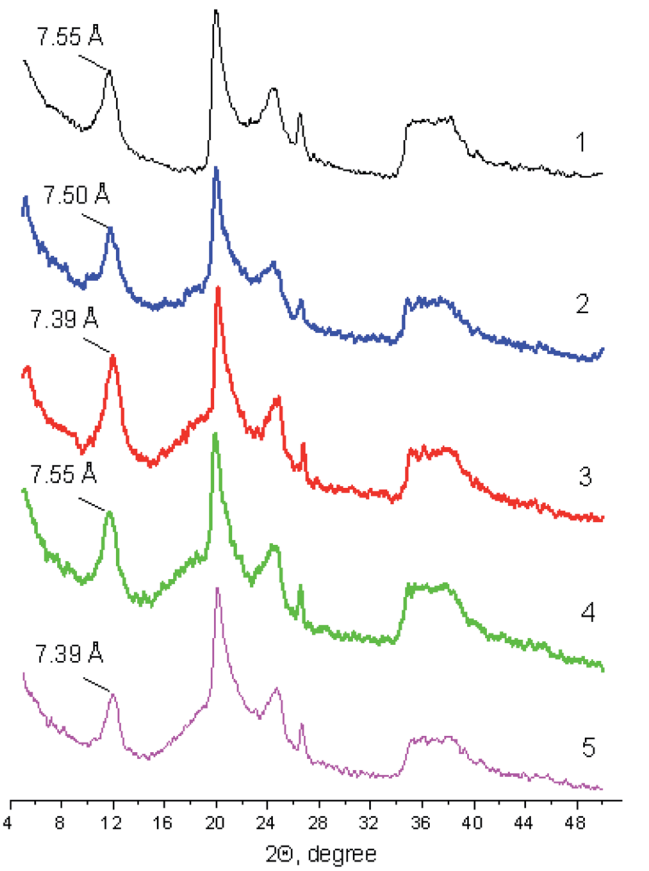

Fig. 2 Diffraction patterns of halloysite (1) and ionogels (2–5) containing ionic liquids: BMImTFSI (2), BMPyrrTFSI (3), BMPipTFSI (4) and $MOc_3AmTFSI$ (5).

were made in an argon atmosphere. The accuracy of the mass and temperature measurements was $\pm 10^{-5}$ g and ± 0.1 °C, respectively. The enthalpy of the phase transition was calculated as follows: $\Delta H = \Delta H^{exp}\ \alpha\ M_w$, where ΔH^{exp} (J g^{-1}) is the experimental value of the heat, α is the IL mass fraction in the ionogel (Table 1), and M_w is the IL molecular weight.

The crystal structure of the clays and composites was studied by the X-ray diffraction method within the angle range of $2\theta = 5$–$50°$ with a DRON-UM1 diffractometer (Russia), CuKα-radiation, $\lambda = 0.154$ nm, operating voltage of 40 kV, current of 40 mA. The scan rate was 0.5 ° min^{-1}.

The FT-IR reflection spectra of the initial ionic liquids and halloysite and the resulting ionogels were registered on a diamond crystal at room temperature using a VERTEX 80v Infrared-Fourier spectrometer with a resolution of 0.2 cm^{-1} (Bruker, Germany) in the range from 500 to 4000 cm^{-1}.

3. Results and discussion

3.1. Structural features

Fig. 2 shows diffraction patterns of halloysite in its initial state and as part of the ionogel prepared. It is evident that the ionic liquids do not have a significant effect on the basal peak position and characteristics. We have earlier reported the value of the basal spacing in the halloysite under study that was equal to 7.55 Å,[45] which is typical of the structure of the partially dehydrated halloysite nanotube form (7 Å).[50] It is shown that the basal spacing in Hal either remains completely unchanged or decreases a little as a result of the solvostatic pressure of ILs, as well as due to the removal of the water initially absorbed on the outer and inner surfaces of the nanotubes. The effect of basal spacing narrowing in clays as a result of the interaction with ionic liquids, in our opinion, is the extreme case of clay swelling inhibition in aqueous suspensions containing high electrolyte concentrations.

3.2. Thermal stability

Thermal stability of ionic liquids in ionogels is one of the key properties for industrial application of these materials. Low thermal stability can lead to failure or deterioration of the functional properties in devices using ionic liquids. In contrast, high thermal stability makes it possible to increase the upper limit of working temperatures of such devices.

It was shown that the decomposition temperature (T_d) of individual ionic liquids depends on the anion type, increasing

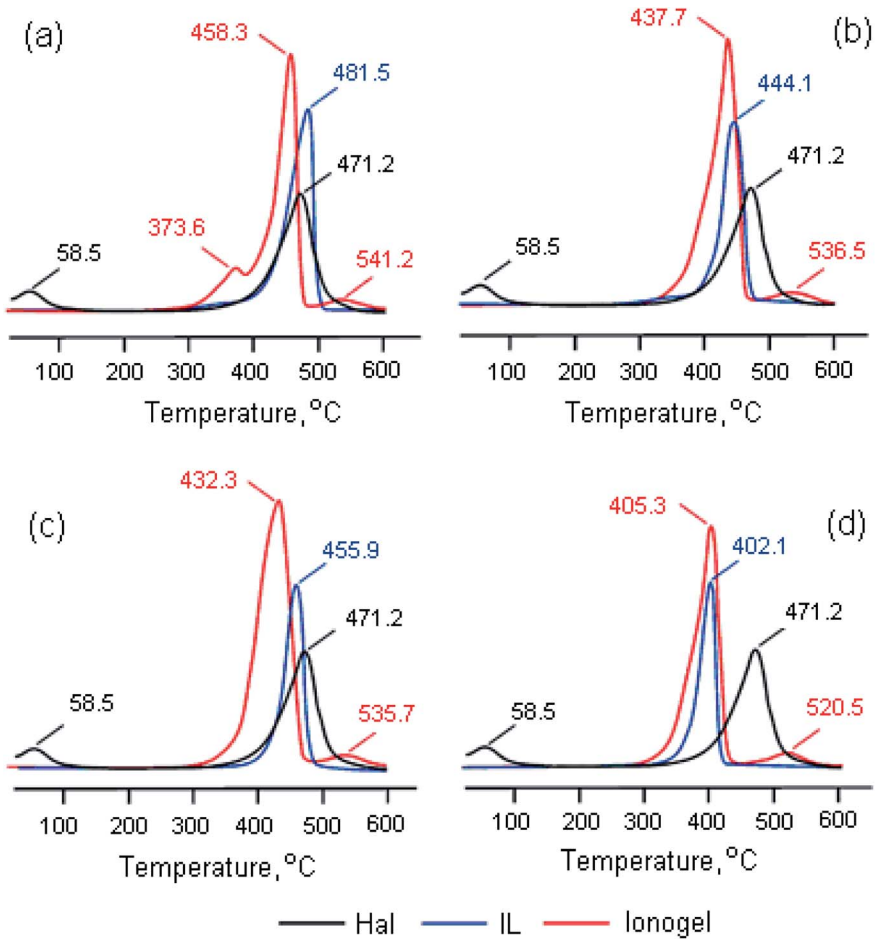

Fig. 3 Differential thermogravimetric curves of halloysite, BMImTFSI (a), BMPipTFSI (b), BMPyrrTFSI (c), and $Moc_3AmTFSI$ (d) ionic liquids and ionogels based on them.

with its size.[51–53] It is also discussed how the cation nature affects the thermal stability of ionic liquids. For example, review[54] summarizes and discusses data on thermal stability of ILs with a $TFSI^-$ anion and different cations. It was established that T_d goes down in the cation series: $BMIm^+$ > $BMPyrr^+$ > $BMPip^+$. However, it is noted that the correlation between the decomposition temperature and IL cation type can hardly be predicted and, for example, in one of the experiments, the salt with a pyrrolidinium cation has higher thermal stability than that with an imidazolium one.

In the adsorbed state, the T_d values can significantly decrease on metal oxide substrates. It was observed, for example, in 1-butyl-3-methylimidazolium hexafluorophosphate adsorbed on SiO_2,[55] where T_d went down from 425 °C to 315 °C. A similar effect of the adsorbent on T_d was observed in work[56] for 1-methyl-3-octylimidazolium hexafluorophosphate that decomposed in the bulk at 350 °C and when it was adsorbed on SiO_2, TiO_2 and γ-Al_2O_3, it decomposed at 310, 215 and 195 °C, respectively. The interactions between the IL and metal oxides, as well as IL solidification on metal oxides,[57,58] evidently, have a considerable effect on the thermal stability limits of the organic salt in these systems.

Fig. 3 shows differential thermogravimetric curves of the considered ionic liquids, halloysite and ionogels based on these compounds. It can be seen that the process of thermal decomposition of the samples under study consists of several stages. The onset and end temperatures (T_{onset} and T_{end}) and the weight loss (Δm) at each stage are presented in Table 2. In the Hal case, the first peak at a temperature of 58.5 °C corresponds to the removal of the physically adsorbed water, the second peak at a temperature of 471.2 °C corresponds to clay dehydroxylation. The process of decomposition of pure ionic liquids consists of one stage. The first peak on the DTG curves of the ionogels with BMPipTFSI, MOc_3AmTFSI and BMPyrrTFSI reflects the IL decomposition, whereas the second – Hal dehydroxylation. Thermal decomposition of BMImTFSI in the presence of HNTs is a two-stage process (with two mass loss peaks); the third peak on this DTG curve corresponds to halloysite dehydroxylation. The presence of two stages of thermocatalytic decomposition of imidazolium ILs in the ionogels, as review[59] shows, can be caused by removal of hydrocarbon substituents at the first stage and decomposition of the cyclic amine – at the second one. It is evident that the bulky imidazolium IL is the most thermally stable among the considered salts with a TFSI-$^-$anion, which agrees with the data in work.[54] The IL thermolysis in the ionogels is observed at other temperatures; however, this change is not one-directional: the peak temperature goes down by 23.4, 23.6, 6.4 °C for the salts with $BMIm^+$, $BMPip^+$, $BMPyrr^+$ cations respectively, and increases by 3.2 °C for the salt with an MOc_3Am^+ cation (Fig. 3). It should be said that in the salts with an imidazolium cation and DCA^- and OTf^- anions that we had studied earlier, we also observed lower thermal stability in the presence of halloysite,[45] montmorillonite K10 and bentonite.[44,60] We made a suggestion that the thermal stability of the ionic liquid entrapped by halloysite decreased due to the confinement and the effect of the interaction with both the clay wall and the water molecules absorbed by the halloysite.[45] At the same time, the dehydroxylation temperature of halloysite as an ionogel component did not only remain the same but also increased by 40–60 °C.

Thus, the exposure of IL/Hal ionogel to higher temperatures causes halloysite to produce a catalytic effect on the thermal decomposition of ionic liquids, and the onset decomposition temperature (T_d) decreases by 106.5, 40.7, 19.0 and 7.7 °C in $BMIm^+$, $BMPip^+$, $BMPyrr^+$ and MOc_3Am^+, respectively.

Table 2 Decomposition temperature (T_{onset}, T_{end}, °C) and mass loss (Δm, %) of the of pure Hal and [X]TFSI sample and [X]TFSI/Hal ionogels[a]

	First stage			Second stage		
System under study	T_{onset}	T_{end}	Δm	T_{onset}	T_{end}	Δm
Hal	~40	88.3	2.4	425.6	497.7	13.1
BMImTFSI	441.1	491.7	90.4			
BMImTFSI/Hal	334.6	383.0	10.8	517.6	574.8	4.7
	435.9	468.5	43.4			
BMPyrrTFSI	432.1	468.6	99.6			
BMPyrrTFSI/Hal	391.4	453.8	57.9	513.2	567.4	4.0
BMPipTFSI	419.6	460.5	99.9			
BMPipTFSI/Hal	400.6	453.6	56.2	510.5	569.5	4.2
MOc_3AmTFSI	377.2	411.7	98.1			
MOc_3AmTFSI/Hal	369.5	419.3	54.1	495.1	547.5	6.4

[a] T_{onset} is the onset temperature, T_{end} is the end temperature.

3.3. DSC studies

Fig. 4 shows the DSC curves of [X]TFSI (X = $BMIm^+$, $BMPyrr^+$, $BMPip^+$ and MOc_3Am^+) ionic liquids in bulk and confined in halloysite. The following types of phase transitions are observed: glass transition (T_g), when a compound transforms from the glass state into the "supercooled liquid" phase, exothermic cold crystallization or devitrification (T_{cc}) (crystallization on cooling), exothermic "solid–solid" phase transition

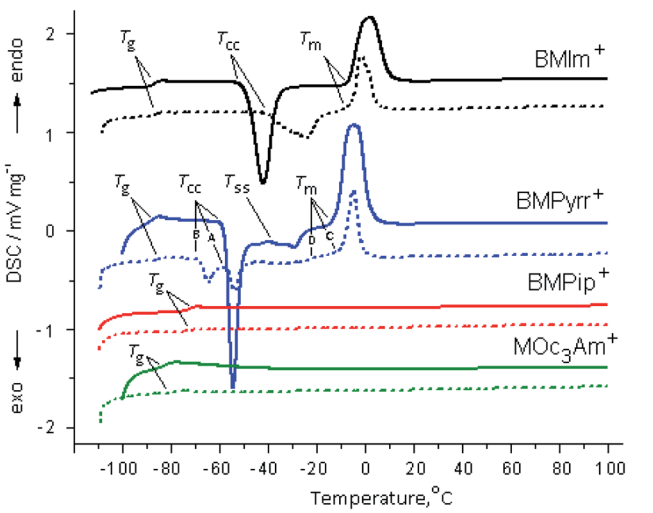

Fig. 4 DSC heating curves of the second cycle of the pure [X]TFSI ionic liquids (solid line) and [X]TFSI/Hal ionogels (dashed line).

(T_{ss}) and endothermic melting (T_m). The phase behavior of the bulk BMPipTFSI and $MOc_3AmTFSI$ ionic liquids is characterized by the formation of the amorphous glass phase only. The phase behavior of the bulk BMImTFSI and BMPyrrTFSI ILs is typical of polymorphic compounds owing to the combination of a small cation and a $TFSI^-$ anion, which has the property of *cis–trans* isomerism.[53,61,62] It was found that the ability to crystallize decreases in the following order: $BMIm^+ > BMPyrr^+$.[63]

The confined ionic liquids have the same phase transitions as the bulk ones (Fig. 4). This behavior is typical of an ionic liquid excess, when its molecules are located both on the surface and inside the pores of the inorganic host matrix.[64–66] The phase transition temperatures, as well as the correctly calculated values of the enthalpy (ΔH_{cc} and ΔH_m) and entropy (ΔS_m) for the bulk and confined ionic liquids, found taking into account the IL content in the ionogel, are given in Table 3. For the bulk ILs, the obtained values are consistent with the literature data.[53,67–71]

It follows from the presented data that the glass transition temperature of the ionic liquids confined in halloysite increases compared to that of the bulk IL by the values of ΔT_g (°C) ($\Delta T_g = T_g^{conf} - T_g^{bulk}$) equal to 1.5, 2.4, 1.5 and 8.0 for $BMIm^+$, $BMPyrr^+$, $BMPip^+$ and MOc_3Am^+, respectively. This feature can be explained by the change in the amorphous phase of the confined ionic liquid due to interaction with halloysite and was also observed in EMImTFSI and $EMImBF_4$ encapsulated in SC2A carbon.[64] The ΔT_g value is higher in MOc_3Am^+ due to the hydrophobic interactions of long octyl chains. Since no events except glass transition were observed in confined $BMPip^+$ and MOc_3Am^+, their phase behavior will not be discussed further. The evident difference between the confined and bulk ionic liquids is the change in the freezing and melting points. At the same time, confinement of the two other ionic liquids in halloysite has a significant effect on the cold crystallization and melting (Fig. 4).

When $BMIm^+$ is captured by halloysite, the T_{cc} and T_m temperatures shift to higher values by 8.5 and 2.0 °C, respectively. The same trend is observed for the melting point determined as the peak point during the first and second heating cycles.[45] This feature can be explained by the structural transformation of the chaotically distributed ions in the bulk phase into an ordered arrangement inside the halloysite nanotubes, which leads to the anomalous phase transition from the liquid to crystallites with higher crystallization and melting temperatures.[59,72,73] It should be noted that the π–π stacking of imidazolium rings is an additional factor in the formation of the more ordered structure of the $BMIm^+$ ionic liquid.

The DSC curve of confined $BMPyrr^+$ has two separate exothermic peaks with the onset temperature T_{cc} (A) and T_{cc} (B), as well as the multiplex endothermic sharp peak at T_m (C) and a weak wave at T_m (D), and there is no exothermic transition T_{ss} (Fig. 4). As in case of $BMIm^+$, T_{cc} (A) ($\Delta T_{cc} = T_{cc}^{conf} - T_{cc}^{bulk}$) increases by 1.0 °C and T_m (C) ($\Delta T_m = T_m^{conf} - T_m^{bulk}$) by 2.1 °C, while the values of T_{cc} (C) and T_m (D) decrease by 9.7 and 14.2 °C, respectively. The depression in the melting point is explained by the interaction of the confined IL with the pore wall.[65,66,74] The $TFSI^-$ anion is mainly adsorbed on the positively charged inner surface of halloysite, which weakens the interaction between the cation and the anion. In this case, some of the ions are included in the rotating motion, and the melting point decreases. The *cis*-conformer is obviously better adsorbed on the wall surface than the *trans*-conformer due to its structure and ability to form more hydrogen bonds. The endothermic wave T_m (D) at −25.5 °C can be attributed to the low-melting mesophase of the *cis*-conformer, while the T_m (C) at −9.2 °C corresponds to the *trans*-conformer of the anion. This assumption is consistent with the infrared data presented below on the tendency towards changes in the equilibrium of the $TFSI^-$ anion *cis*–trans isomers in the studied ionogel series. In addition, it is known that the anion adopts a transoid conformation in the crystalline phase of the low-melting BMImTFSI ionic liquid.[70]

Thus, the DSC data show that the phase behavior of the confined ionic liquids in the studied ionogels is similar to the

Table 3 Thermodynamic parameters of phase transitions of bulk and confined [X]TFSI in Hal (second heating, 10 °C min^{-1})[a]

	BMImTFSI		BMPyrrTFSI		BMPipTFSI		$MOc_3AmTFSI$	
Parameter	Bulk[b]	Con[b]	Bulk	Conf	Bulk	Conf	Bulk	Conf
M_w/g mol^{-1}	419.37		422.41		436.43		648.85	
T_g/°C	−87.7	−86.2	−87.1	−84.7	−73.1	−71.6	−86.6	−78.6
T_{cc}/°C	−48.6	−40.1	−57.5	−56.5 (A)[c]				
				−67.2 (B)[c]				
ΔH_{cc}/kJ mol^{-1}	−19.6	−15.2	−16.1	−4.1 (A)[c]				
				−3.1 (B)[c]				
T_{ss}/°C			−40.0					
ΔH_{ss}/kJ mol^{-1}			−2.6					
T_m/°C	−6.5	−4.5	−11.3	−9.2 (C)[c]				
				−25.5 (D)[c]				
ΔH_m/kJ mol^{-1}	18.8	16.0	26.5	20.7 (C + D)[c]				
ΔS_m/J mol^{-1} K^{-1}[d]	68.3	59.6	101.2	83.6 (C + D)[c]				

[a] T_g is the glass transition (midpoint). T_{cc} is the cold crystallization (onset point). T_{s-s} is the solid–solid transition (onset point). T_m is the melting (onset point). [b] is the first heating. [c] (A), (B), (C), (D) are the onset points in Fig. 4. [d] $\Delta S = \Delta H/T$.

phase behavior of the bulk ionic liquids. At the same time, the change in the phase transition temperatures depends on the cation type. It was found that when the ionic liquid was confined in halloysite, the melting point decreased by about 14 °C for BMPyrrTFSI and increased by about 2 °C for the BMImTFSI ionic liquid.

3.4. FT-IR spectra

The selected regions of the initial halloysite, initial ionic liquids – [X]TFSI and [X]TFSI/Hal ionogels are shown in Fig. 5. The ionogel spectra show vibration bands of both halloysite and ionic liquids, indicating the formation of a hybrid compound.

The bands of pure ILs were identified and assigned in accordance with the literature.[75–80] When [X]TFSI was captured by halloysite, all the νC–H stretching modes of the cation, such as ν(C–H)ar from the aromatic ring and ν(C–H)al from the aliphatic hydrocarbon chains, remained unaffected (Fig. 5a). The weak bands between 1400 and 1600 cm^{-1} (Fig. 5b), which are attributed to different frequency modes of the cation, such as bending δCH_2, δCH_3, rocking rNC2-H, rNCH, νNCN and stretching νC=C, νCHN, νCH_3CN types,[76,77] changed noticeably.

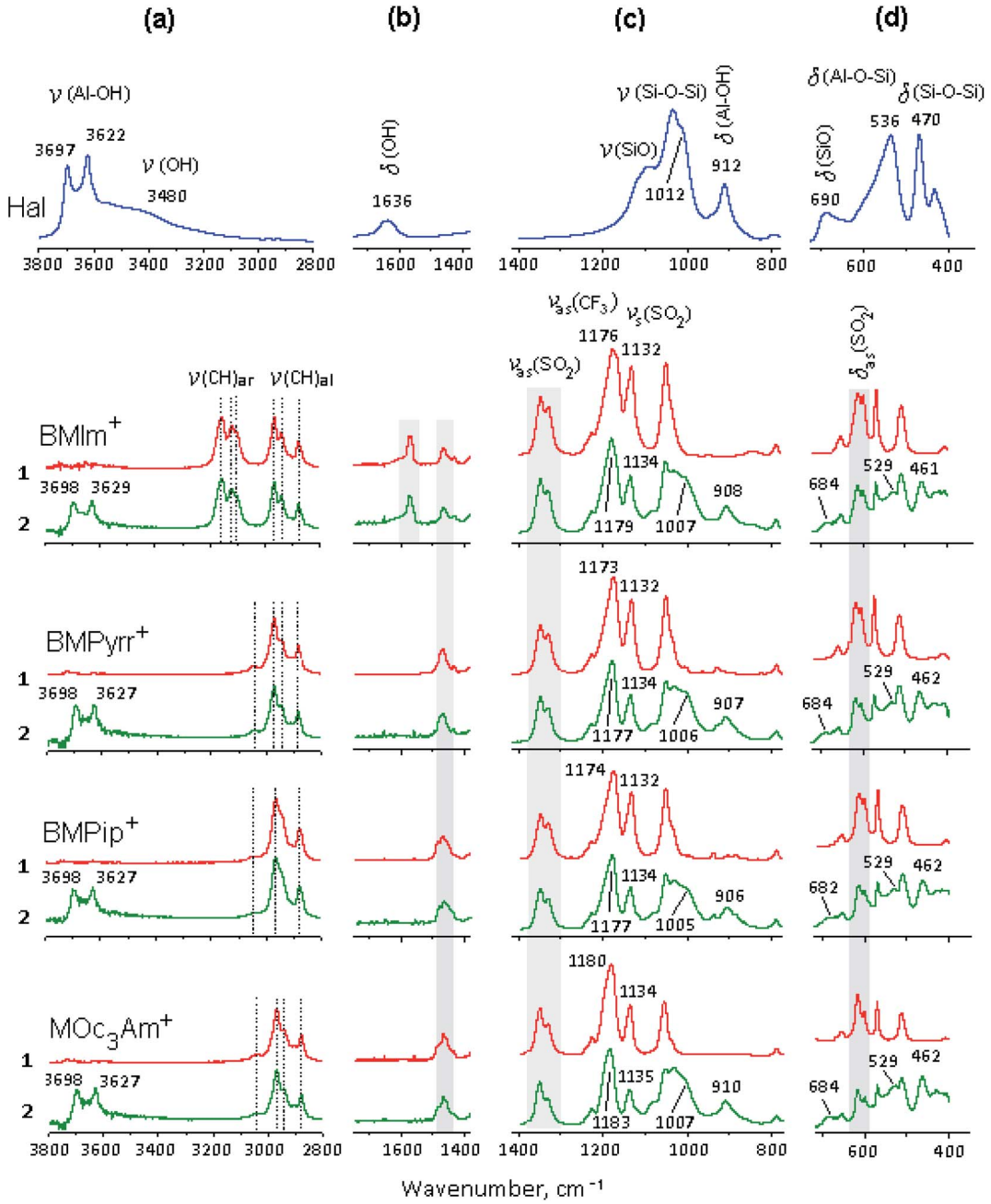

Fig. 5 Selected regions of FTIR reflection spectra of Hal, [X]TFSI (1) and [X]TFSI/Hal (2) between (a) 3800 and 2800 cm^{-1}, (b) 1700 and 1400 cm^{-1}, (c) 1400 and 800 cm^{-1} and (d) 700 and 400 cm^{-1}. The spectra are shifted for convenience.

As Fig. 6a and b shows, new peaks and blue shifts ~1 to 2 cm^{-1} were clearly observed in confined ionic liquids. The stretching modes $\nu_{as}CF_3$ and ν_sSO_2 of the $TFSI^-$ anion also exhibit blue-shifts in the spectra of all the ionogels (Fig. 5c). Such spectral perturbations can be the result of both interactions with clay and altered interactions within the ionic liquid itself due to the confinement effect.

A careful study of the $\delta_{as}SO_2$ bending mode showed that two peaks at 600 and 610 cm^{-1} (Fig. 5d), which correspond to the *cis*- and *trans*-conformers of the $TFSI^-$ anion, respectively,[62,75,78–80] demonstrate redistribution of intensity (I) in favor of the trans isomer (Fig. 6 c). It was found that the I_{trans}/I_{cis} ratio in the ionogel increased compared to that of pure IL by 19, 16, 15 and 5% for $BMIm^+$, $BMPyrr^+$, $BMPip^+$ and MOc_3Am^+, respectively. This indicates that the *trans*-conformer amount in the ionic liquid confined by halloysite depends on the cation structure.

The bands of pure halloysite were identified and assigned in accordance with the literature data.[81–83] The main differences between the spectral bands of the initial halloysite and ionogels are as follows: (i) both bands at 3480 and 1636 cm^{-1}, attributed to the OH stretching and H–O–H bending vibrations of the surface-absorbed H_2O, respectively, almost disappeared due to the decrease in the amount of "free" water; (ii) the peak at 3622 cm^{-1} from the inner OH hydroxyl, in contrast to the peak at 3697 cm^{-1} from the inner-surface OH hydroxyl, blue-shifted significantly, and the I_{3622}/I_{3697} ratio decreased in comparison with that of pure halloysite by 9, 10, 8 and 18% for $BMIm^+$, $BMPyrr^+$, $BMPip^+$ and MOc_3Am^+, respectively, indicating a lower amount of the interlayer water; (iii) all the halloysite bands in the range <1400 cm^{-1} were significantly shifted towards lower frequencies, apparently, due to the non-covalent bonding of the corresponding functional groups.[84] Fig. 7 shows the main shifts of fundamental frequencies of the halloysite and ionic liquids observed in the ionogel spectra.

It follows from the presented data that the [X]TFSI ionic liquid confined by halloysite replaces the water absorbed on the outer and inner surfaces of the halloysite tubes. Halloysite dehydration changes in the following order: $BMIm^+ \sim BMPyrr^+ \sim BMPip^+ << MOc_3Am^+$. It can be assumed that the trapped ionic liquids were mainly located on the outer wall of the halloysite nanotubes, and also partially enclosed in their inner cavity. To confirm that the ionic liquid was encapsulated in nanotubes, the ionogel samples were washed three times with ethyl alcohol[85] then dried under vacuum. In the IR spectra of the washed samples, the frequencies of both the cation and the anion of the studied ionic liquids were observed. An addition, according to TG, the amount of the ionic liquid encapsulated into nanotubes was found to be about 2% of the sample weight.

Inside nanotubes, the ionic liquid is retained due to electrostatic interactions of the $TFSI^-$ anion with the positively charged inner aluminol (–Al–OH) surface, as well as due to hydrogen bonds (CF, SO···HO–Al). In this case, the $TFSI^-$ anion mainly adopts a *sic*-conformation. On the outer wall of the

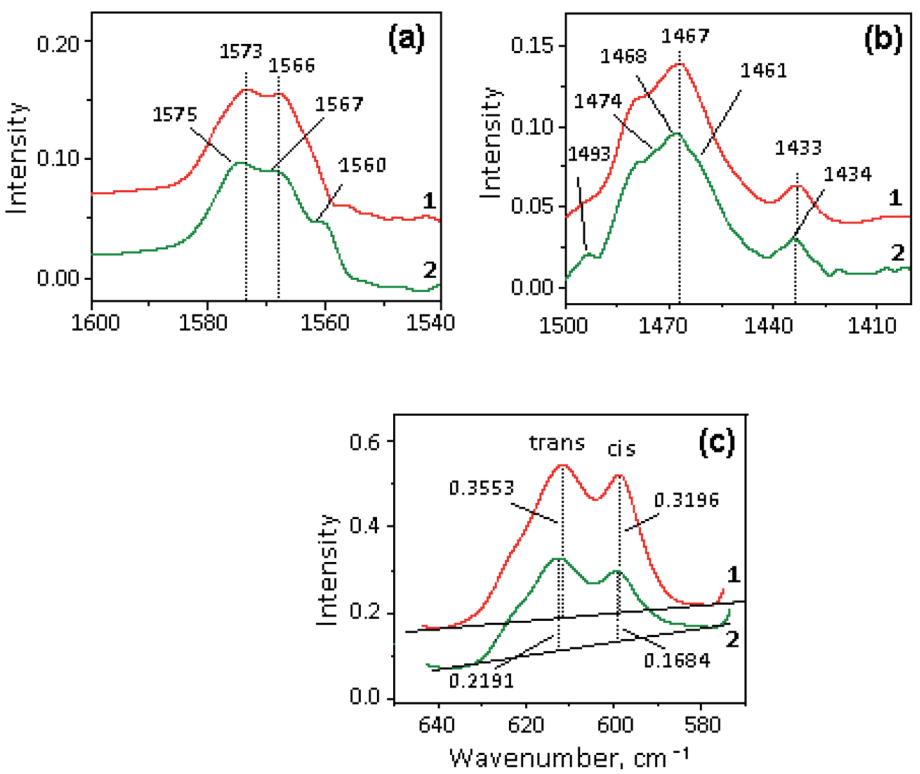

Fig. 6 Infrared spectra of (1) [X]TFSI and (2) [X]TFSI/Hal in the range of (a) 1600–1540 cm^{-1} assigned to νNCN, rNC2-H, νC=C and rNCH; (b) 1500–1400 cm^{-1} assigned to δCH_2, δCH_3, νCHN, νCH_3CN; (c) 640–580 cm^{-1} of the $\delta_{as}SO_2$ mode; X = $BMIm^+$ (a and c), $BMPyrr^+$ (b). The spectra are shifted for convenience.

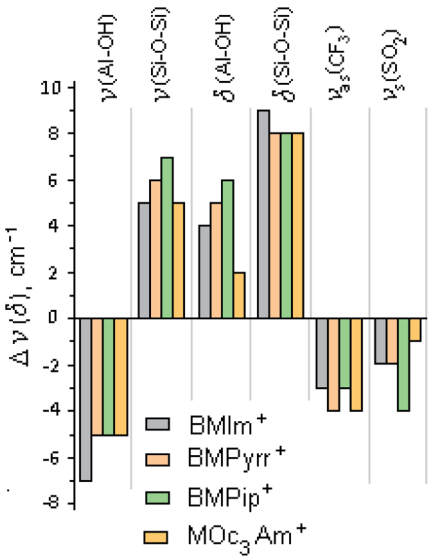

Fig. 7 Histogram of the frequency shifts of Hal and [X]TFSI, $\Delta\nu^{i}(\delta)^{i} = \nu^{i}(\delta)^{i}$ (pure Hal, pure IL) $- \nu^{i}(\delta)^{i}$ (ionogel).

halloysite nanotubes, the $[X]^{+}$ cation interacts with the negatively charged outer siloxane (–Si–O–Si–) surface through electrostatic and hydrogen bonds (CH···OSi). The structure ionic trapped by halloysite could be also change due to weakening or strengthening of inter- and intramolecular interactions of the ionic liquid.[45,86,87] Inside nanotubes, an ionic liquid can self-assemble, forming a pseudocrystalline structure. In this case, the $TFSI^{-}$ anion mainly adopts a *trans*-conformation, and this tendency, depending on the cation type, changes in the following order: $BMIm^{+} > BMPyrr^{+} \sim BMPip^{+} >> MOc_3Am^{+}$.

4. Conclusion

In this work, we obtained ionogels based on BMImTFSI, BMPyrrTFSI, BMPipTFSI and MOc_3Am (~55%) ionic liquids and nanotube halloysite (~45%) by mechanically mixing the components with subsequent degassing at 80 °C in order to reach the maximum degree of filling the tubular halloysite space with ionic liquids. The formation of ionogels is caused by electrostatic and hydrogen interactions of the cation (CH···OSi) and the anion (CF···HO–Al, SO···HO–Al) with halloysite and results in the removal of the water initially absorbed on the outer and inner surfaces of the nanotubes, which leads to lower basal spacing in the halloysite. It was shown that the IL thermal stability in the ionogels decreases as a result of the Hal thermocatalytic effect, and their thermal decomposition represents a one-stage process (ILs with $BMPyrr^{+}$, $BMPip^{+}$, and MOc_3Am^{+} cations) or a two-stage process (BMImTFSI).

In the confined geometry of halloysite, the structure and phase behavior of the studied ionic liquids depends on the cation type and size. An IR spectroscopy study showed that the ratio of the *cis*/*trans* conformers of the $TFSI^{-}$ anion changes in favor of the *trans* conformation in the following order: $BMIm^{+} > BMPyrr^{+} \sim BMPip^{+} >> MOc_3Am^{+}$. This finding is consistent with the DSC data that the confined $BMIm^{+}$ ionic liquid forms a structured phase, predominantly from the transoid $TFSI^{-}$ isomer, with the cold crystallization and melting temperatures higher than in the bulk one, and this ability is weaker in polymorphic $BMPyrr^{+}$. The latter also forms a less structured phase, predominantly from the cisoid $TFSI^{-}$ isomer, with the temperature of cold crystallization and melting lower than in the bulk IL. The larger ionic liquids – $BMPip^{+}$ and MOc_3Am^{+} - exist mainly in the amorphous phase, which becomes more structured inside the halloysite, especially in MOc_3Am^{+} due to three long octyl chains. The presented results suggest a different location and structural organization of the cation and anion of the studied ionic liquids on the inner and outer surfaces of halloysite nanoscrolls and can be of use when developing high-temperature electrochemical devices with quasi-solid electrolytes based on ILs and halloysite clay.

Author contributions

A. V. Agafonov: conceptualization, data curation, funding acquisition, project administration, writing – original draft, writing – review & editing; L. M. Ramenskaya: formal analysis, writing – original draft, writing – review & editing; E. P. Grishina: conceptualization, data curation, formal analysis, writing – original draft, writing – review & editing; N. O. Kudryakova: formal analysis, investigation, visualization, writing – review & editing.

Conflicts of interest

There are no conflicts of interest to declare.

Acknowledgements

This work was funded by the Russian Foundation for Basic Research, project no. 18-29-12012 mk and by State Assignment of the Ministry of Science and Higher Education of the Russian Federation no. AAAA-A21-121011490059-5. The authors would like to express gratitude to the Center for Joint Use of Scientific Equipment "The Upper Volga Region Centre of Physico-Chemical Research".

References

1 J. D. Holbrey and K. R. Seddon, *Clean Prod. Process.*, 1999, **1**, 223–236, DOI: 10.1007/s100980050036.
2 R. D. Rogers and K. R. Seddon, *Science*, 2003, **302**, 792–793, DOI: 10.1126/science.1090313.
3 M. Deetlefs, M. Fanselow and K. R. Seddon, *RSC Adv.*, 2016, **6**, 4280–4288, DOI: 10.1039/c5ra05829e.
4 R. Hayes, G. G. Warr and R. Atkin, *Chem. Rev.*, 2015, **115**, 6357–6426, DOI: 10.1021/cr500411q.
5 N. V. Plechkova and K. R. Seddon, *Chem. Soc. Rev.*, 2008, **37**, 123–150, DOI: 10.1039/B006677J.
6 K. Ueno, K. Hata, T. Katakabe, M. Kondoh and M. Watanabe, *J. Phys. Chem. B*, 2008, **112**, 9013–9019, DOI: 10.1021/jp8029117.

7 Z. He and P. Alexandridis, *Phys. Chem. Chem. Phys.*, 2015, **17**, 18238–18261, DOI: 10.1039/c5cp01620g.
8 A. I. Horowitz and M. J. Panzer, *J. Mater. Chem.*, 2012, **22**, 16534–16539, DOI: 10.1039/c2jm33496h.
9 F. Borghi and A. Podestà, *Adv. Phys.: X*, 2020, **5**, 1736949, DOI: 10.1080/23746149.2020.1736949.
10 Y. L. Verma, A. K. Tripathi, N. Shalu, V. K. Singh, L. Balo, H. Gupta, S. K. Singh and R. K. Singh, *Mater. Sci. Eng., B*, 2017, **220**, 37–43, DOI: 10.1016/j.mseb.2017.03.010.
11 X. Chen, B. Put, A. Sagara, K. Gandrud, M. Murata, J. A. Steele, H. Yabe, T. Hantschel, M. Roeffaers, M. Tomiyama, H. Arase, Yu. Kaneko, M. Shimada, M. Mees and P. M. Vereecken, *Sci. Adv.*, 2020, **6**, eaav3400, DOI: 10.1126/sciadv.aav3400.
12 I. Bou-Malham and L. Bureau, *Soft Matter*, 2010, **6**, 4062–4065, DOI: 10.1039/c0sm00377h.
13 M. Zhao, L. Wei, Y. Zheng, M. Liu, J. Wang and Y. Qiu, *Sci. Total Environ.*, 2019, **666**, 858–864, DOI: 10.1016/j.scitotenv.2019.02.297.
14 A. V. Agafonov and E. P. Grishina, *Russ. J. Inorg. Chem.*, 2019, **64**, 1641–1648, DOI: 10.1134/S0036023619130023.
15 E. Andrzejewska, A. Marcinkowska and A. Zgrzeba, *Polymery*, 2017, **62**, 344–352, DOI: 10.14314/polimery.2017.344.
16 N. Chen, H. Zhang, L. Li, R. Chen and S. Guo, *Adv. Energy Mater.*, 2018, **8**, 1702675, DOI: 10.1002/aenm.201702675.
17 G. K. Dedzo and C. Detellier, *Adv. Funct. Mater.*, 2017, **28**, 1703845, DOI: 10.1002/adfm.201703845.
18 M. Massaro, R. Noto and S. Riela, *Molecules*, 2020, **25**, 4863, DOI: 10.3390/molecules25204863.
19 L. Lisuzzo, G. Cavallaro, S. Milioto and G. Lazzara, *Appl. Clay Sci.*, 2020, **185**, 105416, DOI: 10.1016/j.clay.2019.105416.
20 V. Bertolino, G. Cavallaro, S. Milioto and G. Lazzara, *Carbohydr. Polym.*, 2020, **245**, 116502, DOI: 10.1016/j.carbpol.2020.116502.
21 G. Cavallaro, S. Milioto, S. Konnova, G. Fakhrullina, F. Akhatova, G. Lazzara, R. Fakhrullin and Y. Lvov, *ACS Appl. Mater. Interfaces*, 2020, **12**, 24348–24362, DOI: 10.1021/acsami.0c05252.
22 M. Du, B. Guo and D. Jia, *Polym. Int.*, 2010, **59**, 574–582, DOI: 10.1002/pi.2754.
23 E. Rozhina, S. Batasheva, R. Miftakhova, X. Yan, A. Vikulina, D. Volodkin and R. Fakhrullin, *Appl. Clay Sci.*, 2021, **205**, 106041, DOI: 10.1016/j.clay.2021.106041.
24 Y. Yang, Y. Chen, F. Leng, L. Huang, Z. Wang and W. Tian, *Appl. Sci.*, 2017, **7**, 1215, DOI: 10.3390/app7121215.
25 C. Bretti, S. Cataldo, A. Gianguzza, G. Lando, G. Lazzara, A. Pettignano and S. Sammartano, *J. Phys. Chem. C*, 2016, **120**, 7849–7859, DOI: 10.1021/acs.jpcc.6b01127.
26 N. G. Veerabadran, R. R. Price and Y. M. Lvov, *Nano*, 2007, **2**, 115–120, DOI: 10.1142/S1793292007000441.
27 W. Ma, H. Wu, Y. Higaki and A. Takahara, *Chem. Rec.*, 2018, **18**, 986–999, DOI: 10.1002/tcr.201700093.
28 J. Le Bideau, L. Viau and A. Vioux, *Chem. Soc. Rev.*, 2011, **40**, 907–925, DOI: 10.1039/c0cs00059k.
29 S. Perkin, L. Crowhurst, H. Niedermeyer, T. Welton, A. M. Smith and N. N. Gosvami, *Chem. Commun.*, 2011, **47**, 6572–6574, DOI: 10.1039/c1cc11322d.
30 B. D. Fitchett and J. C. Conboy, *J. Phys. Chem. B*, 2004, **108**(52), 20255–20262, DOI: 10.1021/jp0471251.
31 A. M. Smith, K. R. J. Lovelock, N. N. Gosvami, P. Licence, A. Dolan, T. Welton and S. Perkin, *J. Phys. Chem. Lett.*, 2013, **4**, 378–382, DOI: 10.1021/jz301965d.
32 M. P. Singh, R. K. Singh and S. Chandra, *Prog. Mater. Sci.*, 2014, **64**, 73–120, DOI: 10.1016/j.pmatsci.2014.03.001.
33 S. Marion, S. J. Davis, Z.-Q. Wu and A. Radenovic, *Nanoscale*, 2020, **12**, 8867–8874, DOI: 10.1039/D0NR01164A.
34 El H. Lahrar, A. Belhboub, P. Simon and C. Merlet, *ACS Appl. Mater. Interfaces*, 2020, **12**, 1789–1798, DOI: 10.1021/acsami.9b16740.
35 W. D. Amith, J. J. Hettige, E. W. Castner and C. J. Margulis, *J. Phys. Chem. Lett.*, 2016, **7**, 3785–3790, DOI: 10.1021/acs.jpclett.6b01763.
36 Y.-L. Wang, B. Li, S. Sarman, F. Mocci, Z.-Y. Lu, J. Yuan, A. Laaksonen and M. D. Fayer, *Chem. Rev.*, 2020, **120**, 5798–5877, DOI: 10.1021/acs.chemrev.9b00693.
37 B. Guo, X. Liu, W. Y. Zhou, Y. Lie and D. Jia, *J. Macromol. Sci., Part B: Phys.*, 2010, **49**, 1029–1043, DOI: 10.1080/00222341003609823.
38 M. L. Du, B. C. Guo and D. M. Jia, *Eur. Polym. J.*, 2006, **42**, 1362–1369, DOI: 10.1016/j.eurpolymj.2005.12.006.
39 N. Ning, Q. Yin, F. Luo, Q. Zhang, R. Du and Q. Fu, *Polymer*, 2007, **48**, 7374–7384, DOI: 10.1016/j.polymer.2007.10.005.
40 T. S. Gaaz, A. B. Sulong, A. A. H. Kadhum, A. A. Al-Amiery, M. H. Nassir and A. H. Jaaz, *Molecules*, 2017, **22**, 838, DOI: 10.3390/molecules22050838.
41 M. Soheilmoghaddam, M. U. Wahit, S. Mahmoudian and N. A. Hanid, *Mater. Chem. Phys.*, 2013, **141**, 936–943, DOI: 10.1016/j.matchemphys.2013.06.029.
42 E. Bischoff, D. A. Simon, H. S. Schrekker, M. Lavorgna, L. Ambrosio, S. A. Liberman and R. S. Mauler, *Eur. Polym. J.*, 2016, **82**, 82–92, DOI: 10.1016/j.eurpolymj.2016.07.003.
43 M. Watanabe, M. L. Thomas, S. Zhang, K. Ueno, T. Yasuda and K. Dokko, *Chem. Rev.*, 2017, **117**, 7190–7239, DOI: 10.1021/acs.chemrev.6b00504.
44 E. P. Grishina, L. M. Ramenskaya, N. O. Kudryakova, K. V. Vagin, A. S. Kraev and A. Agafonov, *J. Mater. Res. Technol.*, 2019, **8**, 4387–4398, DOI: 10.1016/j.jmrt.2019.07.050.
45 A. V. Agafonov, N. O. Kudryakova, L. M. Ramenskaya and E. P. Grishina, *Arabian J. Chem.*, 2020, **13**, 9090–9104, DOI: 10.1016/j.arabjc.2020.10.033.
46 A. V. Agafonov, E. P. Grishina, N. O. Kudryakova, L. M. Ramenskaya, A. S. Kraev and V. D. Shibaeva, *Arabian J. Chem.*, 2021, **15**, 103470, DOI: 10.1016/j.arabjc.2021.103470.
47 E. Abdullayev, R. Price, D. Shchukin and Y. Lvov, *ACS Appl. Mater. Interfaces*, 2009, **1**, 1437–1443, DOI: 10.1021/am9002028.
48 L. Lisuzzo, G. Cavallaro, P. Pasbakhsh, S. Milioto and G. Lazzara, *J. Colloid Interface Sci.*, 2019, **547**, 361–369, DOI: 10.1016/j.jcis.2019.04.012.
49 L. Lisuzzo, G. Cavallaro, S. Milioto and G. Lazzara, *J. Nanostruct. Chem.*, 2021, DOI: 10.1007/s40097-021-00391-z.

50 V. A. Drits, B. A. Sakharov and S. Hillier, *Clay Miner.*, 2018, **53**, 691–720, DOI: 10.1180/clm.2018.57.
51 H. L. Ngo, K. LeCompte, L. Hargens and A. B. McEwen, *Thermochim. Acta*, 2000, **97–102**, 357–358, DOI: 10.1016/S0040-6031(00)00373-7.
52 J. Huddleston, A. Visser, W. Reichert, H. Willauer, G. Broker and R. Rogers, *Green Chem.*, 2001, **3**, 156–164, DOI: 10.1039/b103275p.
53 C. P. Fredlake, J. M. Crosthwaite, D. G. Hert, S. N. V. K. Aki and J. F. Brennecke, *J. Chem. Eng. Data*, 2004, **49**, 954–964, DOI: 10.1021/je034261a.
54 E. Siedlecka, M. Czerwicka, S. Stolte and P. Stepnowski, *Curr. Org. Chem.*, 2011, **15**, 1974–1991, DOI: 10.2174/138527211795703630.
55 L. Rodriguez-Perez, Y. Coppel, I. Favier, E. Teuma, P. Serp and M. Gomez, *Dalton Trans.*, 2010, **39**(32), 7565–7568, DOI: 10.1039/c0dt00397b.
56 J. Lemus, J. Palomar, M. Gilarranz and J. J. Rodriguez, *Adsorption*, 2011, **17**, 561–571, DOI: 10.1007/s10450-011-9327-5.
57 A. Mudring, *Aust. J. Chem.*, 2010, **63**, 544–564, DOI: 10.1071/ch10017.
58 A. K. Gupta, Y. L. Verma, R. K. Singh and S. Chandra, *J. Phys. Chem. C*, 2014, **118**, 1530–1539, DOI: 10.1021/jp408142a.
59 S. Zhang, J. Zhang, Y. Zhang and Y. Deng, *Chem. Rev.*, 2017, **117**, 6755–6833, DOI: 10.1021/acs.chemrev.6b00509.
60 O. Alekseeva, A. Noskov, E. Grishina, L. Ramenskaya, N. Kudryakova, V. Ivanov and A. Agafonov, *Materials*, 2019, **12**, 2578, DOI: 10.3390/ma12162578.
61 E. Gómez, N. Calvar and A. Domínguez, *Thermal Behaviour of Pure Ionic Liquids, in Ionic Liquids – Current State of the Art*, IntechOpen, 2015, pp. 199–228, DOI: 10.5772/59271.
62 Y. U. Paulechka, G. J. Kabo, A. V. Blokhin, A. S. Shaplov, E. I. Lozinskaya, D. G. Golovanov, K. A. Lyssenko, A. A. Korlyukov and Y. S. Vygodskii, *J. Phys. Chem. B*, 2009, **113**, 9538–9546, DOI: 10.1021/jp903702c.
63 L. M. Ramenskaya, E. P. Grishina and N. O. Kudryakova, *J. Mol. Liq.*, 2020, **312**, 113368, DOI: 10.1016/j.molliq.2020.113368.
64 F. Béguin, V. Pavlenko, P. Przygocki, M. Pawlyta and P. Ratajczak, *Carbon*, 2020, **169**, 501–511, DOI: 10.1016/j.carbon.2020.07.071.
65 M.-A. Néouze, J. Le Bideau, P. Gaveau, S. Bellayer and A. Vioux, *Chem. Mater.*, 2006, **18**, 3931–3936, DOI: 10.1021/cm060656c.
66 Y. Liu, G. Wu, H. Fu, Z. Jiang, S. Chen and M. Sha, *Dalton Trans.*, 2010, **39**, 3190–3194, DOI: 10.1039/b924042j.
67 D. R. MacFarlane, P. Meakin, N. Amini and M. Forsyth, *J. Phys.: Condens. Matter*, 2001, **13**, 8257–8267, DOI: 10.1088/0953-8984/13/36/303.
68 S. V. Dzyuba and R. A. Bartsch, *ChemPhysChem*, 2002, **3**, 161–166, DOI: 10.1002/1439-7641(20020215)3.
69 H. Tokuda, K. Hayamizu, K. Ishii, M. A. B. H. Susan and M. Watanabe, *J. Phys. Chem. B*, 2005, **109**, 6103–6110, DOI: 10.1021/jp044626d.
70 A. R. Choudhury, N. Winterton, A. Steiner, A. I. Cooper and K. A. Johnson, *J. Am. Chem. Soc.*, 2005, **127**, 16792–16793, DOI: 10.1021/ja055956u.
71 E. Gómez, N. Calvar, Á. Domínguez and E. A. Macedo, *Ind. Eng. Chem. Res.*, 2013, **52**, 2103–2110, DOI: 10.1021/ie3012193.
72 J. Im, S. D. Cho, M. H. Kim, Y. M. Jung, H. S. Kim and H. S. Park, *Chem. Commun.*, 2012, **48**, 2015–2017, DOI: 10.1039/c2cc16367e.
73 S. Chen, G. Wu, M. Sha and S. Huang, *J. Am. Chem. Soc.*, 2007, **129**, 2416–2417, DOI: 10.1021/ja067972c.
74 M. Kanakubo, Y. Hiejima, K. Minami, T. Aizawa and H. Nanjo, *Chem. Commun.*, 2006, **17**, 1828–1830, DOI: 10.1039/b600074f.
75 F. M. Vitucci, F. Trequattrini, O. Palumbo, J.-B. Brubach, P. Roy and A. Paolone, *Vib. Spectrosc.*, 2014, **74**, 81–87, DOI: 10.1016/j.vibspec.2014.07.014.
76 S. A. Katsyuba, E. E. Zvereva, A. Vidiš and P. J. Dyson, *J. Phys. Chem. A*, 2007, **111**, 352–370, DOI: 10.1021/jp064610i.
77 N. E. Heimer, R. E. Del Sesto, Z. Meng, J. S. Wilkes and W. R. Carper, *J. Mol. Liq.*, 2006, **124**, 84–95, DOI: 10.1016/j.molliq.2005.08.004.
78 A. M. Moschovi, S. Ntais, V. Dracopoulos and V. Nikolakis, *Vib. Spectrosc.*, 2012, **63**, 350–359, DOI: 10.1016/j.vibspec.2012.08.006.
79 M. Shukla, H. Noothalapati, S. Shigeto and S. Saha, *Vib. Spectrosc.*, 2014, **75**, 107–117, DOI: 10.1016/j.vibspec.2014.10.006.
80 I. Rey, P. Johansson, J. Lindgren, J. C. Lassègues, J. Grondin and L. Servant, *J. Phys. Chem. A*, 1998, **102**, 3249–3258, DOI: 10.1021/JP980375V.
81 J. T. Kloprogge, Characterisation of Halloysite by Spectroscopy, in *Developments in Clay Science, Halloysite and Imogolite*, 2016, ch. 6, pp. 115–136, doi: DOI: 10.1016/B978-0-08-100293-3.00006-6.
82 P. Yuan, Thermal-Treatment-Induced Deformations and Modifications of Halloysite, in *Developments in Clay Science, Halloysite and Imogolite*, 2016, pp. 137–166. doi: DOI: 10.1016/b978-0-08-100293-3.00007-8.
83 H. Cheng, R. L. Frost, J. Yang, Q. Liu and J. He, *Spectrochim. Acta, Part A*, 2010, **77**, 1014–1020, DOI: 10.1016/j.saa.2010.08.039.
84 N. Zhao, Y. Liu, X. Zhao and H. Song, *Nanoscale*, 2016, **8**, 1545–1554, DOI: 10.1039/c5nr06888f.
85 J. M. Crosthwaite, S. N. V. K. Aki, E. J. Maginn and J. F. Brennecke, Liquid Phase Behavior of Imidazolium-Based Ionic Liquids with Alcohols, *J. Phys. Chem. B*, 2004, **108**, 5113–5119, DOI: 10.1021/jp037774x.
86 L. M. Ramenskaya and E. P. Grishina, *J. Mol. Liq.*, 2016, **218**, 133–137, DOI: 10.1016/j.molliq.2016.02.037.
87 T.-H. Wang, E.-Y. Lin and H.-C. Chang, *Nanomaterials*, 2019, **9**, 620, DOI: 10.3390/nano9040620.